Chinese Journal of Structural Chemistry xxx (xxxx) xxx

Contents lists available at ScienceDirect

Chinese Journal of Structural Chemistry

journal homepage: www.journals.elsevier.com/chinese-journal-of-structural-chemistry

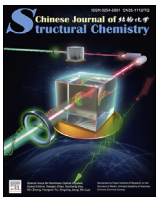

Article

Ultra-long room temperature phosphorescence, intrinsic mechanisms and application based on host-guest doping systems

Jianmei Guo [a,1], Yupeng Zhao [b,1], Lei Ma [b,**], Yongtao Wang [a,*]

[a] College of Chemistry and Bioengineering, Guilin University of Technology, Guilin, 541004, PR China
[b] Tianjin International Center for Nanoparticles and Nanosystem, Tianjin University, Tianjin, 300072, PR China

ARTICLE INFO

Keywords:
Room-temperature phosphorescence
Host-guest doping
Isomer
Benzocarbazole
Polymorphism

ABSTRACT

To construct efficient room-temperature phosphorescence (RTP) doping systems by simple doping methods, isomers 2-(2-(9H-carbazol-9-yl)benzyl)malononitrile (o-CzCN), 2-(3-(9H-carbazol-9-yl)benzyl)malononitrile (m-CzCN) and 2-(4-(9H-carbazol-9-yl)benzyl)malononitrile (p-CzCN) were designed and synthesized by choosing commercial carbazole. Based on the structure-function relationships of three isomers and excellent compatibility between carbazole and benzocarbazole, 2-(3-(9H-carbazol-9-yl)benzyl)malononitrile (Lm-CzCN) and 2-(3-(5H-benzo[b]carbazol-5-yl)benzyl)malononitrile (m-BCzCN) were prepared by self-made carbazole and 2-naphthylamine. Then, Lm-CzCN/m-BCzCN was constructed and optimized by dissolution and rapid evaporation, as well as tuning the mass ratios between Lm-CzCN and m-BCzCN. Lm-CzCN shows excitation dependent RTP and afterglow lifetimes, as well as concentration dependent RTP emission in poly(vinyl alcohol) (PVA) films, while 1% m-BCzCN@PVA film emits bright green afterglow, with RTP and afterglow lifetimes of 2.303 and 17 s in turn, as well as RTP quantum yield of 0.22. More importantly, Lm-CzCN/m-BCzCN presents ultra-long room temperature phosphorescence, with RTP and afterglow lifetimes of 597.58 ms and 8 s, respectivley. Moreover, crystals m-CzCN and p-CzCN, as well as Lm-CzCN/m-BCzCN can be excited by visible light of 440 nm, showing yellow afterglow of 1–4 s. Noteworthy, polymorphism o-$CzCN_Y$ and o-$CzCN_B$ were found, whose different emission was investigated by molecular conformation, intermolecular arrangement and stacking patterns. Finally, multiple encryptions were successfully constructed based on the different luminescent properties.

1. Introduction

Ultra-long organic room temperature phosphorescence (UORTP) materials have broad applications in many high-tech fields such as information storage, bioimaging, and anti-counterfeiting due to their low cost, good biocompatibility, and easily tailoring molecular structures [1–7]. Generally speaking, phosphorescence performances of organic luminogens are closely related to molecular structures and surrounding environments [8–12]. Compared to promoting intersystem transitions by molecular design, constructing a rigid environment to inhibit molecular motion plays a more important role in enhancing phosphorescence performance and excavating new phosphorescent materials [13–20]. Currently, crystal engineering and host-guest doping have become two main means to suppress non radiative transitions [21–30]. However, crystal engineering faces drawbacks such as poor repeatability, difficulty in large-scale preparation, and susceptibility to brittleness [31–34]. Owing to flexible selectivity of host and guest materials, constructing host-guest doping systems has become a research hotspot of RTP materials.

The construction methods of host-guest doping system mainly include melting, cocrystal and grinding [35,36]. Among them, most of the efficient host-guest doping systems come from melt blending, which requires host materials to have good crystallinity and lower melting point. Thereby, thermal decomposition of host and guest materials is avoided, and molecular motion and oxygen quenching are suppressed, but the selection range of host materials is limited [37,38]. We know that organic host and guest materials generally can be dissolved in organic solvents. Provided host and guest materials have excellent compatibility, and host materials have strong crystallization ability, efficient host-guest doping systems are expected to be achieved by dissolution/rapid evaporation

* Corresponding author.
** Corresponding author.
E-mail addresses: lei.ma@tju.edu.cn (L. Ma), wyt_shzu@163.com (Y. Wang).
[1] Contributed equally.

https://doi.org/10.1016/j.cjsc.2024.100335
Received 11 April 2024; Received in revised form 7 May 2024; Accepted 11 May 2024

and dissolution/reduced pressure concentration. Commercial carbazole is a natural host-guest doping system, with trace carbazole isomers 1H-benzo[f]indole (B_d). Owing to complex preparation and separation processes for B_d, it is difficult to determine the content of B_d and molecular structures of B_d derivatives after multi-step synthesis reactions, resulting in uncertain structure-function relationships and underlying mechanisms [39–41]. Therefore, carbazole derivatives are gradually becoming forbidden regions that phosphorescent molecule designs are reluctant to touch. Subsequently, benzocarbazole (B_c) was also discovered in commercial carbazole, with shorter synthesis steps and similar doping effects relative to B_d [42]. Meanwhile, carbazole and B_c have excellent compatibility and matching energy levels, which are crucial for achieving efficient room temperature phosphorescence. Furthermore, the reported literature indicated introducing sp^3-methylene linkers in phosphors can form stronger intermolecular interactions, and effectively suppress non-radiative transitions of phosphors [43,44].

As shown in Fig. 1, o-CzCN, m-CzCN, and p-CzCN were designed and synthesized by using commercial carbazole as raw material based on the above-mentioned and isomerization effect. The structure-function relationships of isomers were investigated in detail by photophysical performance testing and crystal analysis. Crystals o-CzCN, m-CzCN, and p-CzCN show UORTP of 242.87, 1018.34, and 991.74 ms as well as long afterglows of 3, 9 and 8 s in turn. Based on the longest RTP and afterglow lifetimes for m-CzCN in three isomers, Lm-CzCN with the same molecular structure of m-CzCN was prepared by self-made carbazole. Then, m-BCzCN was designed and synthesized by using naphthylamine as raw materials. Phosphorescence nature of Lm-CzCN and m-BCzCN was confirmed by time-resolved phosphorescence decay curves and afterglow in DCM solution at 77 K (Fig. S3 and Figs. S7–8), with phosphorescence lifetimes of 287.48 ms for Lm-CzCN as well as 739.37 ms (500 nm) and 783.74 ms (550 nm) for m-BCzCN, lasting afterglows of 8 s. Lm-CzCN/m-BCzCN was constructed by DCM dissolution/rapid evaporation, whose RTP intensity and afterglow lifetime were further optimized by tuning the mass ratio between m-BCzCN and Lm-CzCN from 1:10000 to 1:10. Encouragingly, Lm-CzCN/m-BCzCN shows UORTP at the mass ratios from 1:10000 to 1:100. Among them, 1% Lm-CzCN/m-BCzCN presents RTP of 597.58 ms and afterglows over 7s, confirming the effectiveness of the above molecular design strategy. Moreover, Lm-CzCN shows doping concentration and excitation wavelength dependent afterglow and RTP lifetimes in PVA films, which is important for high-level anti-counterfeiting. More importantly, afterglow and RTP lifetimes of 1% m-BCzCN@PVA film are up to over 17 and 2.304 s in turn, with bright green afterglow and RTP quantum yield (Φ_P) of 0.22. Of note, 1% Lm-CzCN/m-BCzCN, crystals m-CzCN and p-CzCN can emit bright afterglows of 1.0, 4 and 2 s respectively by switching on-off visible light of 440 nm. Besides,

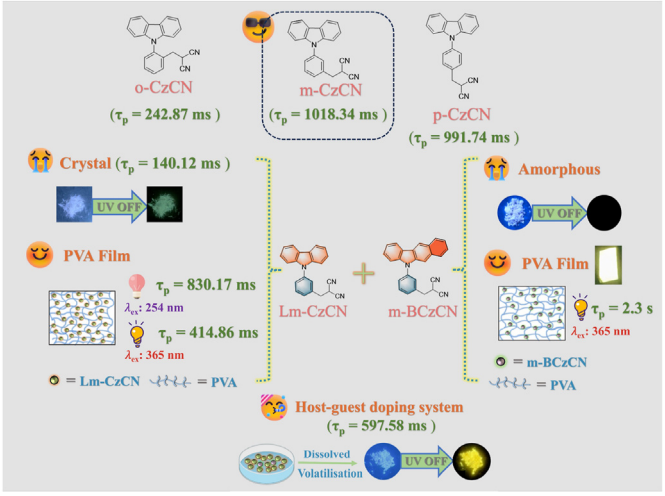

Fig. 1. The main research ideas and performance diagram.

polymorphism o-$CzCN_B$ and o-$CzCN_Y$ were found, with different intensity ratios between fluorescence and RTP, and different RTP lifetimes due to the different molecular conformations.

2. Results and discussion

Isomers o-CzCN, m-CzCN, and p-CzCN were prepared (Scheme S1) starting from commercial carbazole by two step synthesis and characterized by ^{1}H NMR, ^{13}C NMR, HR-MS, high-performance liquid chromatography (HPLC) and X-ray single crystal diffraction (Figs. S20–S33 and Fig. S14). They exhibit similar UV-vis absorption spectra in DCM solution (10^{-5} M), with two absorption bands at 280–300 and 300–350 nm, which are attributed to n-π* and π-π* transition, respectively (Fig. S1). Under 290 nm excitation, o-CzCN only gives bathochromic-shifts of 3 nm compared with m-CzCN and p-CzCN (Fig. S1). With increasing solvent polarity from n-hexane to DMSO, three compounds give positive solvation effect, demonstrating intramolecular charge transfer (ICT) effect (Fig. S1). By slowly evaporating mixed solution (EtOAc/n-hexane, V/V = 1:4) of three isomers, crystals o-CzCN, m-CzCN (CCDC 2346117), and p-CzCN (CCDC 2346118) were obtained. Switching on/off 365 nm UV lamp, the three crystals show light-blue, deep-blue and blue purple fluorescence, as well as yellow-green, yellow and orange afterglow in sequence. Among them, m-CzCN has the longest afterglow time, lasting for 9 s, followed by p-CzCN (8 s) and o-CzCN (2 s) (Fig. 2(b)). The decay spectra indicate that o-CzCN, m-CzCN, and p-CzCN generate multiple emission peaks around 500, 550, and 600 nm, of which the emission peak around 500 nm should be attributed to intrinsic RTP peak of three isomers, while the other two come from trace B_d in commercial carbazole based on the reported literatures [42] (Fig. 2(a)). The RTP characteristics at 500, 550, and 600 nm were further confirmed by the time-resolved phosphorescence decay curves with RTP lifetimes of 242.87 ms for o-CzCN, 373.77, 924.68, and 1018.34 ms for m-CzCN, as well as 421.13, 991.74, and 969.97 ms for p-CzCN correspondingly (Fig. S2). Based on the longest RTP lifetime and the same level of impurity content (Figs. S24, S25, S29 and S33) for m-CzCN in isomers, Lm-CzCN was synthesized using self-made carbazole (Scheme S2), completely eliminating the influence of trace B_d, whose structure and purity were confirmed by ^{1}H NMR, ^{13}C NMR, HR-MS and HPLC (Figs. S34–S37). The previous studies showed that trace B_d hardly affected the molecular spatial conformation, intermolecular arrangement and stacking modes [45]. Therefore, we speculate that m-CzCN and Lm-CzCN should have the same intrinsic RTP peak. By contrast, RTP emission maxima of Lm-CzCN is basically consistent with the intrinsic RTP peak of m-CzCN, further confirming tiny influence of trace B_d on intrinsic RTP of luminogens (Fig. 2(a)). The fluorescence emission spectra indicate that o-CzCN has two emission peaks at 363 and 507 nm, belonging to fluorescence and RTP, respectively. m-CzCN gives single fluorescence peak at 437 nm, while p-CzCN presents three fluorescence peaks at 372, 413, and 437 nm, illustrating generation of multiple singlet states. Of note, fluorescence spectra of Lm-CzCN generate two emission peaks at 387 and 507 nm, corresponding to singlet and triplet emission, which are different from that of m-CzCN due to the absence of energy transfer between Lm-CzCN and B_d/B_d derivative (Fig. 2(a)). Owing to the absence of B_d, Lm-CzCN shows shorter RTP (140.12 ms) and afterglow (2 s) lifetimes than m-CzCN. In DCM solution (10^{-5} M) at 77 K, phosphorescence peaks of o-CzCN, Lm-CzCN, m-CzCN, and p-CzCN are located at 450–463 nm, showing obvious blue shifts in comparison to that of the corresponding crystals because of the reduced intermolecular interactions (Fig. 2(e)). More interestingly, o-CzCN formed two different crystals, emitting blue (o-$CzCN_B$) and yellow (o-$CzCN_Y$) fluorescence, respectively (Fig. 2(f)). Crystal analysis indicates that both crystals own different molecular conformations but almost identical intermolecular interactions and stacking modes (Figs. S14–16). Furthermore, both o-$CzCN_B$ (CCDC 2346116) and o-$CzCN_Y$ present dual-band emission, with small wavelength shifts but high-contrast intensity ratios between RTP (520 nm) and fluorescence (375 nm), as well as different RTP

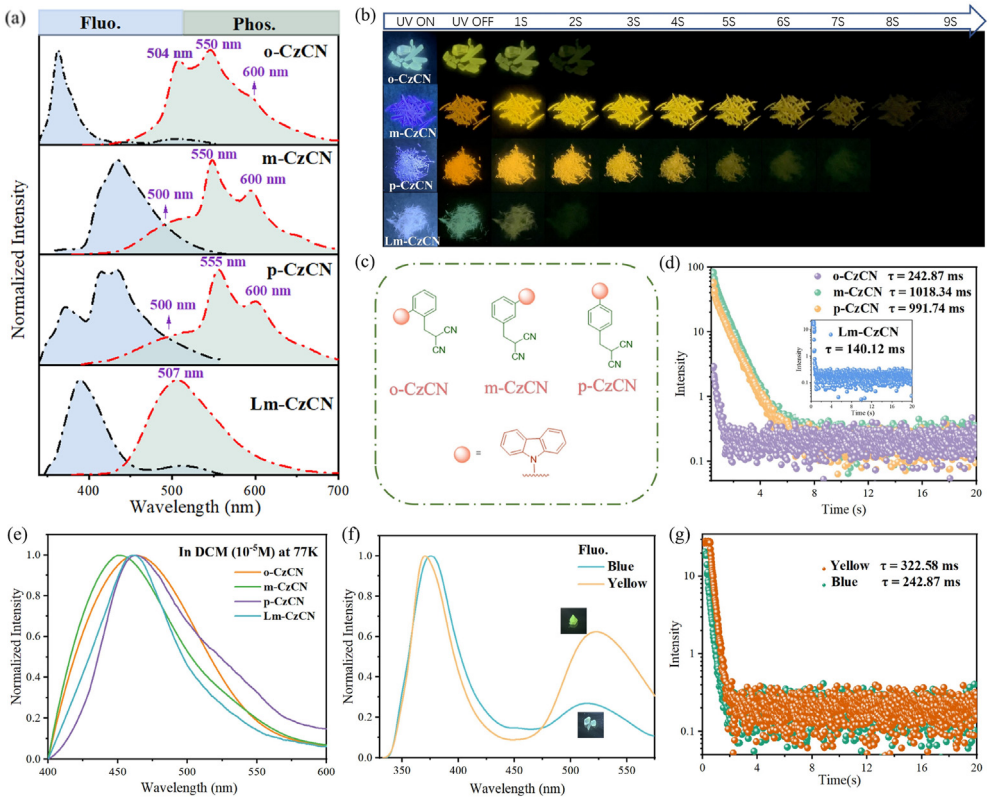

Fig. 2. (a) Fluorescence and phosphorescence emission spectra of o-CzCN, m-CzCN, p-CzCN and Lm-CzCN crystals (delayed time τ_d:1 ms, λ_{ex}:365 nm). (b) Photographs taken before and after irradiation (365 nm) under ambient conditions. (c) Molecular structures of o-CzCN, m-CzCN, p-CzCN. (d) Time-resolved phosphorescence decay curves of o-CzCN, m-CzCN, p-CzCN, and Lm-CzCN excited at 365 nm. (e) Phosphorescence spectra of o-CzCN, m-CzCN, p-CzCN, and Lm-CzCN in DCM (1×10^{-5} M) at 77 K. (f) Fluorescence emission spectra and (g) time-resolved phosphorescence decay curves of polymorphism o-CzCN in different states (τ_d = 1 ms, λ_{ex}:365 nm).

lifetimes (Fig. 2(f and g)). Thereby, fluorescence discrepancy between o-$CzCN_B$ and o-$CzCN_Y$ should be due to the molecular conformation rather than different contents of impurity.

Based on the long RTP lifetime of crystal Lm-CzCN, RTP of Lm-CzCN was further investigated by host-guest doping of polymethyl methacrylate (PMMA)/PVA and Lm-CzCN, whose intensity and lifetime were optimized by tuning mass ratios of Lm-CzCN and PMMA/PVA from 0.2:100, 1:100 to 5:100. Unfortunately, Lm-CzCN@PMMA films always present poor RTP lifetime and afterglow at different doping mass ratios, whose afterglows last for less than 1 s. Compared with PMMA, PVA has stronger intermolecular hydrogen bonds, which can more effectively suppress oxygen diffusion and molecular motion. When the mass ratios of PVA and Lm-CzCN are 0.2:100, 1:100 and 5:100, they are named as 0.2% Lm-CzCN@PVA, 1% Lm-CzCN@PVA, and 5% Lm-CzCN@PVA films in sequence. When Lm-CzCN is replaced with m-BCzCN, the naming follows this rule as well. Three Lm-CzCN@PVA films with different doping concentrations exhibit light- and deep-blue fluorescence respectively under the irradiation of 254 and 365 nm UV lamps (Fig. 3(a)), but with invisible afterglow due to short irradiation time and the presence of oxygen in doping films, which consumes triplet excitons of Lm-CzCN. By photoradiation deoxygenation of 60 s, the doping films give visible or persistent afterglows. Whether under 254 or 365 nm radiation, 1% Lm-CzCN@PVA film displays the longest RTP and afterglow lifetimes, followed by 0.2% Lm-CzCN@PVA and 5% Lm-CzCN@PVA films. The doping concentration dependent RTP results from the few triplet excitons formed at low doping concentrations, while excessive triplet excitons triggered by high concentrations are prone to collision deactivation. By contrast, 0.2% Lm-CzCN@PVA and 1% Lm-CzCN@PVA films show longer RTP and afterglow lifetimes, as well higher Φ_P for 254 nm than 365 nm UV irradiation, but the opposite situation occurs for 5% Lm-CzCN@PVA film (Fig. 3 and Table S2). The former is attributed to the generation of high-energy singlet states under 254 nm excitation, which boosts more intersystem transitions, while the latter lies in the formation of aggregated states, leading to intensified molecular motion and bathochromic shifts of absorption maxima. Noteworthy, RTP and afterglow lifetimes of 1% Lm-CzCN@PVA film are up to 830.17 ms and 8 s separately at the excitation of 254 nm (Fig. 3(a and e)). Furthermore, fluorescence of 0.2% Lm-CzCN@PVA and 1% Lm-CzCN@PVA films is located at 370 nm at the excitation of 365 nm, whereas their RTP emission maxima red shift to 460 nm (Fig. 3(b)), which is consistent with the emission of DCM solution at 77 K, corresponding to the phosphorescence emission of unimolecular Lm-CzCN. Compared with 0.2% Lm-CzCN@PVA and 1% Lm-CzCN@PVA films, RTP emission maxima of 5% Lm-CzCN@PVA film show 47 nm bathochromic-shifts with yellow afterglow, which is consistent with RTP maxima of crystal Lm-CzCN, ascribed to RTP of aggregated Lm-CzCN (Fig. 3(a) and S4). Therefore, it can be inferred that molecular motion can be effectively suppressed when unimolecular Lm-CzCN is uniformly dispersed in PVA film, but not for aggregated Lm-CzCN. As a control, 0.2% m-CzCN@PVA, 1% m-CzCN@PVA, and 5% m-CzCN@PVA films were also prepared. By contrast, 0.2% m-CzCN@PVA and 1% m-CzCN@PVA films show shorter afterglow lifetimes than 0.2% Lm-CzCN@PVA and 1% Lm-CzCN@PVA, but 5% m-CzCN@PVA film relative to Lm-CzCN@PVA film provides an opposite result (Fig. S5). Obviously, trace B_d plays a negative role in afterglow lifetime at low doping concentrations, but with a positive role at high concentrations. As a speculation, the formation of efficient energy transfer/charge separation between m-CzCN and B_d need maintain a certain intermolecular distance between the host and guest molecules.

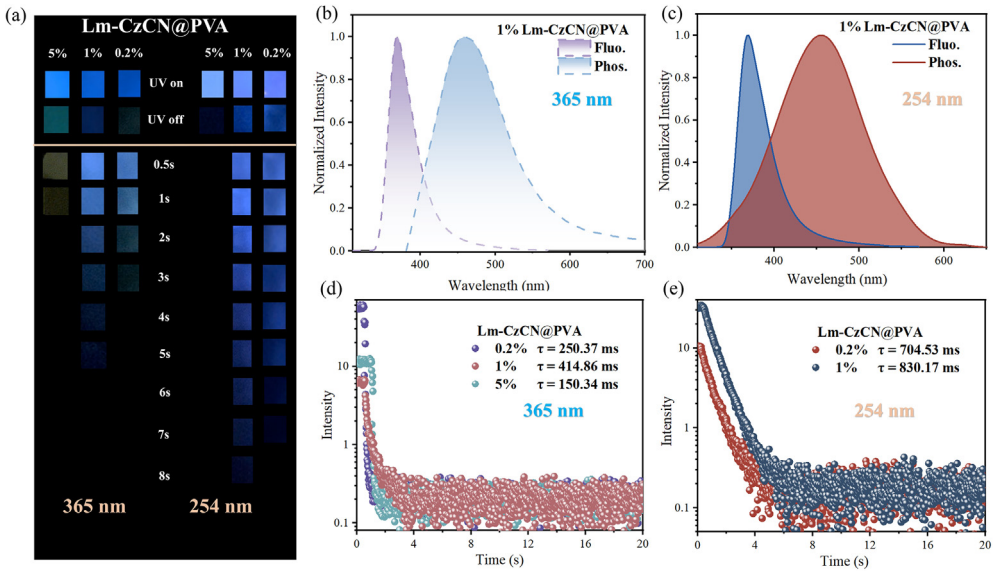

Fig. 3. (a) Photograph of Lm-CzCN@PVA films under 365 and 254 nm UV lamps. Fluorescence and phosphorescence spectra of Lm-CzCN@PVA films excited by 365 nm (b) and 254 nm (c) at different doping concentrations (τ_d = 5 ms). Time-resolved phosphorescence decay curves of Lm-CzCN@PVA films under 365 nm (d) and 254 nm (e) excitation at different doping concentrations (τ_d = 1 ms).

B_d and benzocarbazole were discovered in commercial carbazole one after another, but the former has a more lengthy and complex preparation process than the latter. Combined with the principle of "like dissolves like", m-BCzCN was designed and synthesized by a five-step synthesis reaction (Scheme S3), which was characterized by ^{1}H NMR, ^{13}C NMR, HR-MS, and HPLC (Figs. S38–S41). The fluorescence and RTP emission of m-BCzCN are located at 430 and 600 nm in solid state, respectively. In DCM solution at 77 K, m-BCzCN shows multiple phosphorescence peaks at 500, 550, 600, and 620 nm, but without visible afterglow in solid state (Fig. 4(b)). Owing to longer conjugated structure for m-BCzCN than Lm-CzCN, different Lm-CzCN/m-BCzCN were constructed by using Lm-CzCN and m-BCzCN as host and guest materials respectively, which were optimized by dissolving and rapidly evaporating DCM solution of Lm-CzCN and m-BCzCN at 60 °C, with mass ratios from 10000:1 to 10:1. The results indicate that Lm-CzCN/m-BCzCN presents the strongest RTP emission intensity and the longest RTP lifetime at the mass ratio of 100:1 (Fig. 4(a) and Fig. S6b), with RTP lifetimes of 597.58 and 453.15 ms at 507 and 540 nm in turn (Fig. 4(d)), as well as Φ_P of 0.16 (Table S2). Of note, fluorescence and RTP maxima of Lm-CzCN/m-BCzCN agree well with that of m-BCzCN in DCM solution at 77 K (Fig. 4(c)), demonstrating Lm-CzCN sensitized emission of m-BCzCN and uniform dispersion of m-BCzCN in Lm-CzCN. XRD results of Lm-CzCN, m-BCzCN, and Lm-CzCN/m-BCzCN suggest that Lm-CzCN shows excellent crystallization performance, while m-BCzCN is in an amorphous form (Fig. 4(e)). Even through rapid solvent evaporation, Lm-CzCN/m-BCzCN still displays sharp diffraction signals, basically consistent with that of Lm-CzCN.

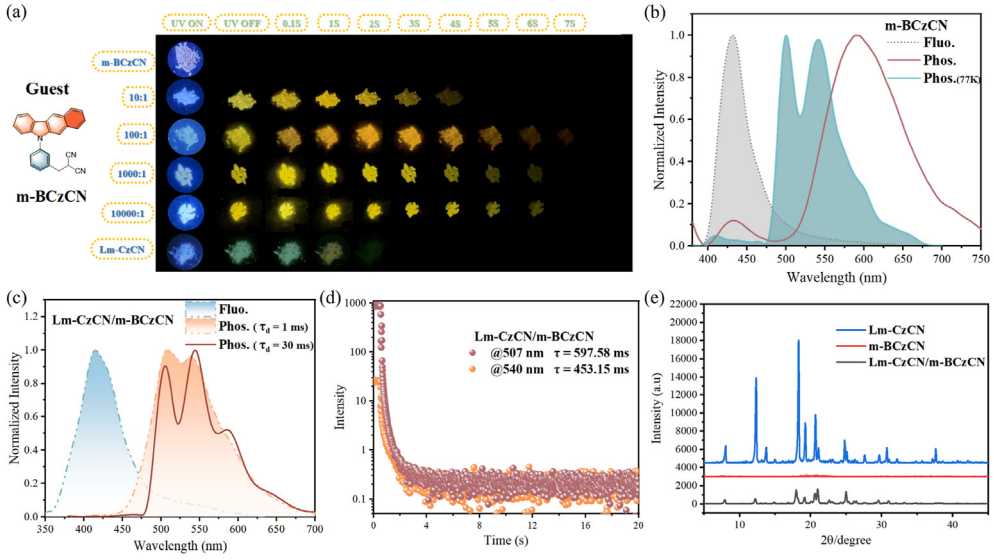

Fig. 4. (a) Photographs under 365 nm light irradiation and turning off the light irradiation of Lm-CzCN/m-BCzCN at optimal doping concentration. (b) Fluorescence and phosphorescence emission spectra of m-BCzCN crystals and DCM solution at 77 K (10^{-5} M). (c) Fluorescence and phosphorescence emission spectra of Lm-CzCN/m-BCzCN (λ_{ex}:365 nm). (d) Time-resolved phosphorescence decay curves of Lm-CzCN/m-BCzCN (τ_d = 1 ms). (e) Corresponding X-ray diffraction patterns of Lm-CzCN, m-BCzCN and Lm-CzCN/m-BCzCN.

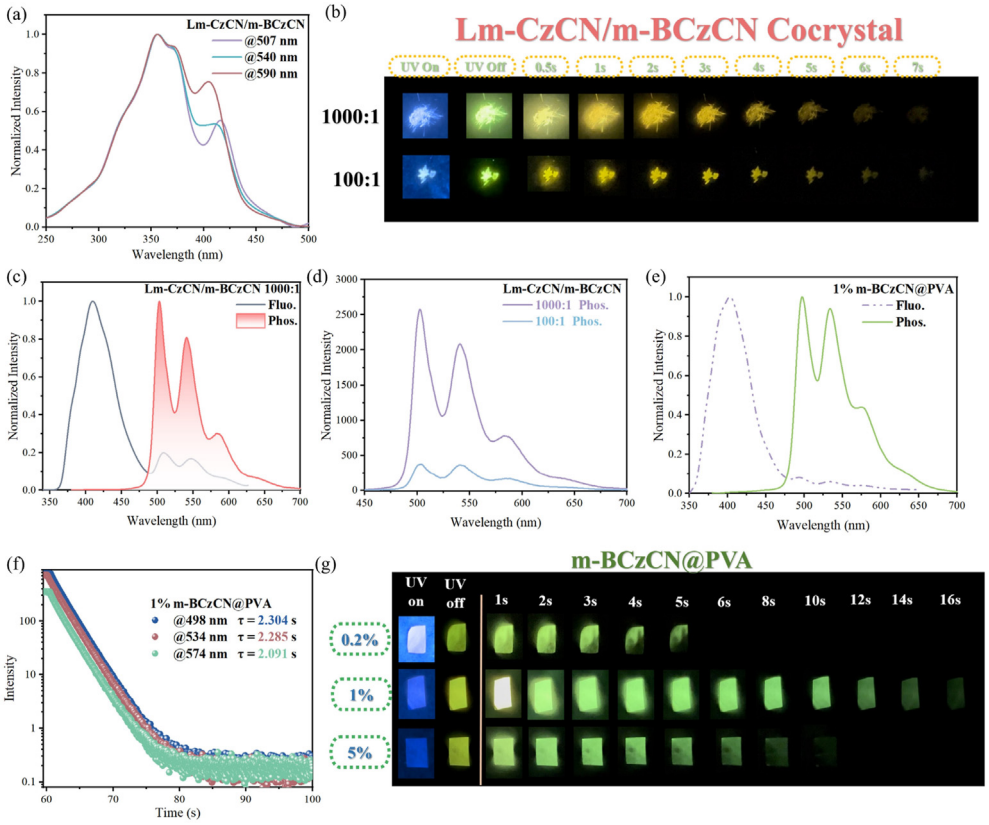

Fig. 5. (a) Excitation spectra of Lm-CzCN/m-BCzCN constructed by rapid solvent evaporation at different emission peaks. (b) Photographs of Lm-CzCN/m-BCzCN constructed by cocrystal at different mass ratios. (c) Fluorescence and phosphorescence emission spectra of Lm-CzCN/m-BCzCN constructed by cocrystal at the mass ratio of 1:1000. (d) Phosphorescence emission spectra of Lm-CzCN/m-BCzCN constructed by cocrystal at the mass ratios of 1:1000 and 1:100. (e) Fluorescence and phosphorescence emission spectra of 1% Lm-CzCN@PVA film. (f) Time-resolved phosphorescence decay curves of 1% Lm-CzCN@PVA film at different emission peaks. (g) Photographs of m-BCzCN@PVA films by the switching on/off of 365 nm lamp.

Furthermore, excitation spectra of Lm-CzCN, m-BCzCN, and Lm-CzCN/m-BCzCN at different RTP emission maxima were provided (Fig. S6), with their excitation peaks located at 348 and 405 nm, 270 and 325 nm, as well as 352, 370 and 405 nm correspondingly (Fig. 5(a)). Overall, Lm-CzCN/m-BCzCN exhibits similar excitation spectra to Lm-CzCN. Moreover, it shows similar excitation spectra at 507, 540 and 590 nm, indicating the existence of mutual conversion between the three energy levels. Beyond expectation, m-BCzCN has longer molecular conjugation than Lm-CzCN, but shorter excitation maxima, which should be attributed to crystalline Lm-CzCN and unimolecular m-BCzCN in

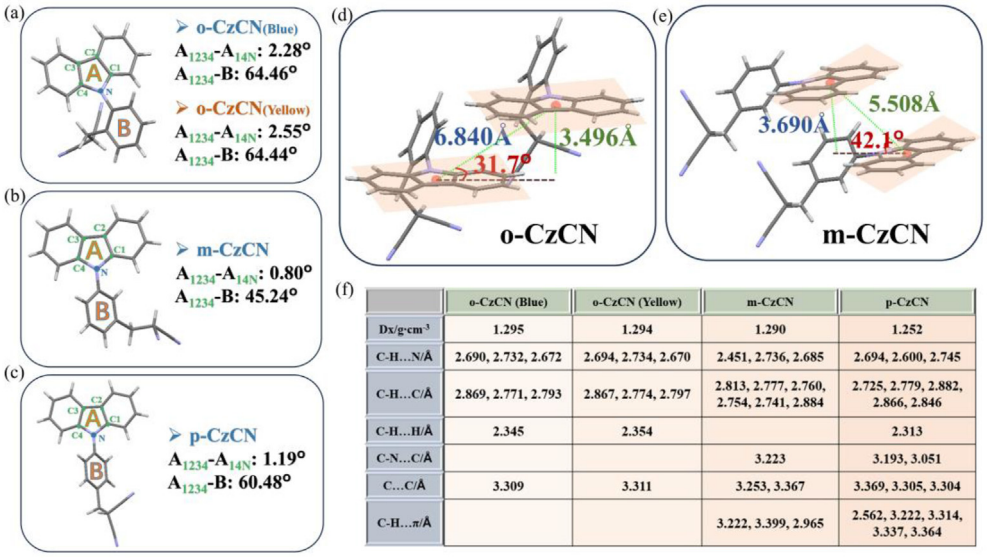

	o-CzCN (Blue)	o-CzCN (Yellow)	m-CzCN	p-CzCN
Dx/g·cm⁻³	1.295	1.294	1.290	1.252
C-H…N/Å	2.690, 2.732, 2.672	2.694, 2.734, 2.670	2.451, 2.736, 2.685	2.694, 2.600, 2.745
C-H…C/Å	2.869, 2.771, 2.793	2.867, 2.774, 2.797	2.813, 2.777, 2.760, 2.754, 2.741, 2.884	2.725, 2.779, 2.882, 2.866, 2.846
C-H…H/Å	2.345	2.354		2.313
C-N…C/Å			3.223	3.193, 3.051
C…C/Å	3.309	3.311	3.253, 3.367	3.369, 3.305, 3.304
C-H…π/Å			3.222, 3.399, 2.965	2.562, 3.222, 3.314, 3.337, 3.364

Fig. 6. The spatial conformations of (a) o-CzCN, (b) m-CzCN and (c) p-CzCN. Intermolecular distances and pitch angles of (d) o-CzAD and (e) m-CzAD. (f) Intermolecular interactions of different compounds.

solution, indicating that ordered molecular stacking and arrangement can prolong the molecular conjugation. Considering that the excitation spectrum of crystalline Lm-CzCN can reach over 450 nm, the afterglows of o-CzCN, m-CzCN, p-CzCN, Lm-CzCN, m-BCzCN, and Lm-CzCN/m-BCzCN were investigated at different excitation wavelengths. As shown in Figs. S9–18, m-CzCN, p-CzCN, and Lm-CzCN/m-BCzCN exhibit bright yellow afterglow, with afterglow lifetimes of 4 s for m-CzCN even under 440 nm excitation. By comparison, afterglow lifetimes of Lm-CzCN/m-BCzCN are noticeably shortened, which should mainly be attributed to the shorter crystal size for Lm-CzCN than m-CzCN due to rapid evaporation. o-CzCN and Lm-CzCN can also emit weak green afterglow under 440 nm excitation, while afterglow of m-BCzCN is invisible under 254–440 nm excitation. Thereby, RTP of Lm-CzCN/m-BCzCN was once again confirmed as host sensitized luminescence. Because amorphous cannot effectively suppress oxygen diffusion and molecular vibration, m-BCzCN shows weak phosphorescence emission and invisible afterglow. For comparison, 1% and 1‰ Lm-CzCN/m-BCzCN were constructed by cocrystal at the mass ratios of 1:100 and 1:1000 in sequence, whose

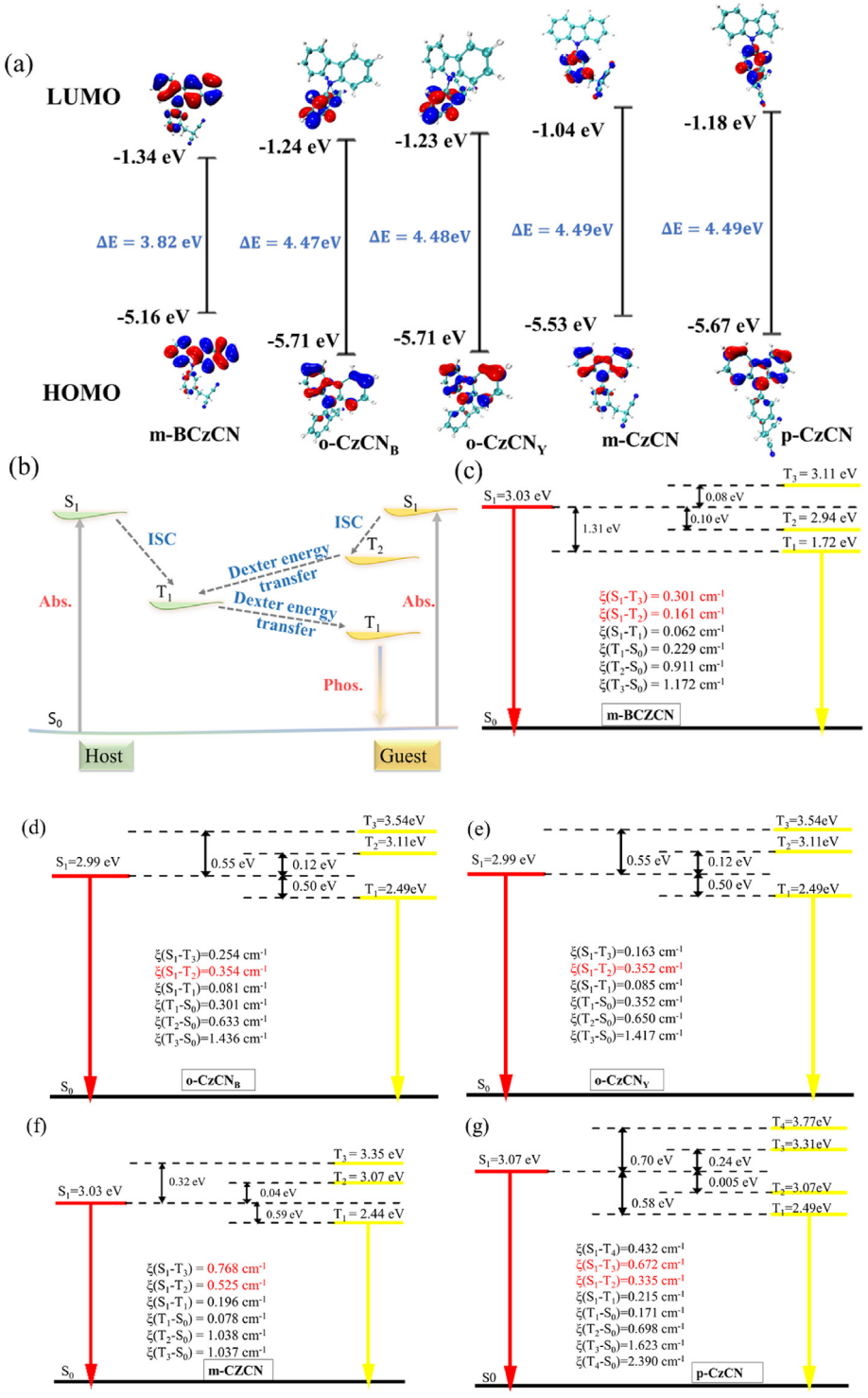

Fig. 7. (a) HOMO and LUMO distributions of m-BCzCN, o-CzCN$_B$, o-CzCN$_Y$, m-CzCN and p-CzCN. (b) Proposed photophysical processes in host-guest doping systems. (c) Energy levels and ξ of m-BCzCN, (d) o-CzCN$_B$, (e) o-CzCN$_Y$, (f) m-CzCN, and (g) p-CzCN.

afterglow lifetimes are equivalent to that of rapid solvent evaporation (Fig. 5(b)). It is worth noting that RTP maxima and excitation spectra of Lm-CzCN/m-BCzCN show slight blue-shifts for cocrystal than rapid evaporation (Fig. 5(c)). Moreover, excitation spectra of 1‰ Lm-CzCN/m-BCzCN relative to 1% Lm-CzCN/m-BCzCN present weaker intensity at above 400 nm (Fig. S6d), illustrating that doping mode and mass ratio influenced emission and excitation spectra of Lm-CzCN/m-BCzCN attributed to different intermolecular interactions between Lm-CzCN/m-BCzCN [46]. In other words, increasing doping mass ratio and rapid solvent evaporation is beneficial for increasing the molecular conjugation of doping systems. More excitingly, 0.2% m-BCzCN@PVA, 1% m-BCzCN@PVA, and 5% m-BCzCN@PVA films emit bright green RTP, with Φ_P of 0.22, afterglow and RTP lifetimes over 16 and 2.3 s respectively for 1% m-BCzCN@PVA film (Fig. 5(f and g) and Table S2). Noteworthy, 1% m-BCzCN@PVA film and Lm-CzCN/m-BCzCN show the same spectral curve, which illustrates unimolecular dispersion of m-BCzCN (Fig. 5(e)). However, RTP peaks of Lm-CzCN/m-BCzCN present obvious bathochromic-shifts compared with those of 1% m-BCzCN@PVA film, thereby emitting yellow RTP due to the different dipole interactions between host and guest materials.

To understand the structure-function relationship of three isomers, molecular conformation, intermolecular interactions, arrangement and stacking modes of o-CzCN, m-CzCN and p-CzCN were investigated. By slow evaporation of the mixed solution of DCM and n-hexane, four crystals were successfully grown. Of note, o-CzCN gives two different crystals with blue and yellow fluorescence respectively, named as o-$CzCN_B$ and o-$CzCN_Y$ in turn. They have completely identical weak intermolecular interaction sites, only with tiny differences in the magnitude of interactions (Fig. 6(f) and Fig. S14). Moreover, they show almost identical dihedral angles between carbazole and benzene ring units. However, o-$CzCN_Y$ (2.55°) maintains a more twisted carbazole unit compared with o-$CzCN_B$ (2.28°) (Fig. 6(a)), which may affect SOC and ISC, leading to the longer RTP lifetime for o-$CzCN_Y$ than o-$CzCN_B$. Compared with crystal o-CzCN, crystals m-CzCN and p-CzCN show stronger and more intermolecular interactions (Fig. 6(f) and Fig. S14). Besides, m-CzCN adopts intermolecular parallel stacking mode (Fig. 6(e) and Fig. S17), with weak intermolecular π-π stacking between carbazole units and high crystal density, while p-CzCN adopts intermolecular antiparallel stacking mode, without weak intermolecular π-π stacking between carbazole units (Fig. S18). Furthermore, crystal m-CzCN shows the most planar molecular conformation in three isomers (Fig. 6(a–c)), which is unfavorable for reducing the energy gap (ΔE_{ST}) between S_1 and triplet excited state (T_1) in theory. In general, high crystal density and more intermolecular interactions contribute to reduce molecular motions, while the weak intermolecular π-π stacking can prolong RTP lifetime, thereby crystal m-CzCN presents the longest RTP and afterglow lifetimes. For crystal o-CzCN, weak intermolecular interactions lead to the shortest RTP and afterglow lifetimes. Owing to more distorted molecular conformation, crystal p-CzCN shows higher Φ_P than m-CzCN (Table S1).

Molecular structures of o-$CzCN_B$, o-$CzCN_Y$, m-CzCN, p-CzCN and m-BCzCN were optimized at the B3LYP/def2-SVP level. Then, the highest occupied molecular orbitals (HOMO) and the lowest unoccupied molecular orbitals (LUMO) distribution, energy level, and spin-orbit coupling constant (ξ)between singlet and triplet states were achieved at the B3LYP/TZVP level. Theoretical calculations indicate that HOMO of m-CzCN is concentrated on the benzene ring rather than carbazole unit (Fig. 7(a)), while LUMO is mainly located on carbazole unit, confirming ICT effect in donor (D)-acceptor (A) type o-$CzCN_B$, o-$CzCN_Y$, m-CzCN, and p-CzCN. The effective ISC process transfers excitons from singlet to triplet states, thereby accumulating enough triplet excitons. To obtain UORTP materials, it is necessary to increase the intersystem transition rate (k_{ISC}) from S_1 to T_n ($n \geq 1$) states, which mainly involves SOC and ΔE_{ST} between S_1 to T_n. m-CzCN only has one T_1 below the S_1 state, with an energy gap of 0.59 eV and ξ of 0.196 cm^{-1}. In literatures [47,48], T_n within a range of 0.3 eV above and below S_1 state were often considered as effective triplet states. Therefore, the large energy gap between S_1 to T_n may be the main reason of weak RTP emission for Lm-CzCN under 365 nm radiation. Besides, $\xi(T_1 \rightarrow S_0)$ of m-CzCN is only 0.078 cm^{-1}, leading to a slow rate of phosphorescence radiation, which is not conducive to compete with non-radiation caused by intramolecular thermal vibration and rotation, and O_2 quenching. Therefore, Lm-CzCN generates RTP in PVA film rather than in crystalline state. Notably, there are two triplet excited states (T_2 and T_3) around the S_1 state, with $\xi(S_1 \rightarrow T_2)$ and $\xi(S_1 \rightarrow T_3)$ of 0.525 and 0.768 cm^{-1} in turn (Fig. 7(c)). When Lm-CzCN is irradiated by 254 nm UV light, electrons transfer to higher-level singlet excited state (S_n, $n > 1$) from ground state (S_0), then back to T_1 via ISC between S_n and T_2, T_3 and Dexter energy transfer ($T_2 \rightarrow T_1$ and $T_3 \rightarrow T_1$), generating more triplet excitons. Thereafter, Lm-CzCN presents higher RTP quantum yield (Φ_P) and lifetime by 254 nm UV radiation (Table S2). By contrast, both HOMO and LUMO of m-BCzCN simultaneously concentrate on the benzcarbazole and benzene rings, with weaker ICT effect for m-BCzCN than Lm-CzCN (Fig. 7(a)). m-BCzCN has tiny ΔE_{S1T2} (0.10 eV) between S_1 and T_2, as well as $\xi(S_1 \rightarrow T_2)$ of 0.161 cm^{-1}, contributing to the rapid generation of triplet excitons. However, large energy gap (1.22 eV) between T_2 (2.94 eV) and T_1 (1.72 eV) isn't conducive to the energy transfer from T_2 to T_1 (Fig. 7(d)). When m-BCzCN is doped in Lm-CzCN, T_1 (2.44 eV) of Lm-CzCN can act as an energy bridge of m-BCzCN between T_2 and T_1 (Fig. 7(b)). As a result, the energy transfer rate is accelerated, reducing the impact of non-radiative energy loss. In PVA film, non-radiative energy loss is also inhibited, leading to persistent and bright afterglow for m-BCzCN. Besides, m-BCzCN has a long molecular conjugation,

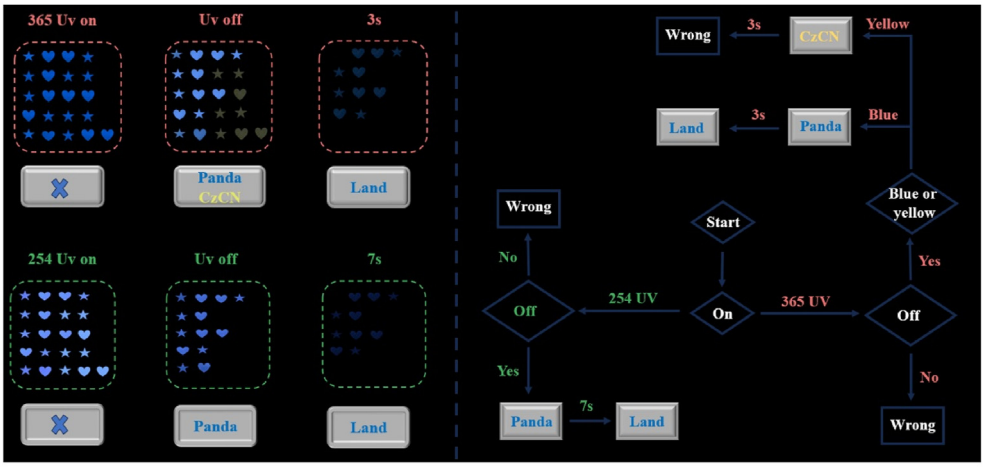

Fig. 8. Information encryption of Lm-CzCN@PVA films by using different excitation wavelengths and doping concentrations.

corresponding to the π→π* transition of $T_1 \rightarrow S_0$, which is forbidden [49]. It favours the slow phosphorescence radiation rate constant (m-BCzCN@PVA, kp = 0.469 s^{-1}), resulting in long-lived phosphorescence. Interestingly, o-$CzCN_B$ and o-$CzCN_Y$ have the same energy levels of singlet and triplet states, as well as almost identical $\xi(S_1 \rightarrow T_2)$ but different $\xi(T_1 \rightarrow S_0)$. Owing to its bigger $\xi(T_1 \rightarrow S_0)$ (0.352 cm^{-1}) than o-$CzCN_B$ (0.301 cm^{-1}), o-$CzCN_Y$ shows relatively stronger RTP, which is consistent with the experimental results. By comparing ξ and energy gaps of three isomers, m-CzCN and p-CzCN can generate more triplet excitons due to small energy gaps between S_1 and T_2, T_3, as well as big $\xi(S_1 \rightarrow T_2)$ and $\xi(S_1 \rightarrow T_3)$. More importantly, $\xi(T_1 \rightarrow S_0)$ of m-CzCN is significantly smaller than that of o-$CzCN_B$, o-$CzCN_Y$, and p-CzCN, resulting in the longest afterglow and RTP lifetimes for m-CzCN in three isomers.

Based on different luminescent characteristics for Lm-CzCN@PVA films, 0.2% Lm-CzCN@PVA, 1% Lm-CzCN@PVA, and 10% Lm-CzCN@PVA films were selected to achieve a high-level information encryption (Fig. 8 and S19). A series of "star" and "heart" patterns were prepared by templates, which were arranged according to some special programs. When illuminated by a 365 nm UV lamp, the patterns emitted deep-blue fluorescence, but failed to give the correct encrypted information by comparing the password table. When the 365 nm lamp was turned off, the above deep-blue patterns presented blue and yellow afterglows, which were decrypted as "Panda" and "CzCN" in sequence. After turning off the 365 nm UV lamp for 3 s, only blue afterglow remained, which were decrypted as "Land". However, the above patterns only showed blue afterglow by the switching on-off of a 254 nm UV lamp, giving encrypted information "Panda", which transformed into "Land" after 7 s due to different RTP lifetimes, presenting a complex program encryption.

3. Conclusions

By introducing malononitrile structural unit via a sp^3-methylene linker, o-CzCN, m-CzCN and p-CzCN were endowed with excellent crystallization ability. Moreover, polymorphism o-$CzCN_Y$ and o-$CzCN_B$ were found with different molecular conformation and identical intermolecular arrangement and stacking patterns. The more twisted carbazole unit leads to stronger RTP emission and longer lifetime for o-$CzCN_Y$ than o-$CzCN_B$. The structure function relationship displays that crystal m-CzCN presents the longest RTP and afterglow lifetimes in three isomers due to strong intermolecular interactions, weak intermolecular π-π stacking, and high crystal density. Owing to excellent crystallization ability of Lm-CzCN and outstanding compatibility of Lm-CzCN and m-BCzCN, as well as matching energy levels between Lm-CzCN and m-BCzCN, host-guest doping systems with ultra-long room temperature phosphorescence lifetimes were achieved via dissolution and rapid evaporation. Lm-CzCN shows excitation dependent RTP and afterglow lifetimes, as well as concentration dependent RTP emission in PVA films, which should be due to ISC between S_n and T_2/T_3 under 254 nm UV radiation. More importantly, 1% m-BCzCN@PVA film emits bright green afterglow, with RTP and afterglow lifetimes of 2.303 and 17 s in turn, as well as Φ_P of 0.22. Last but not least, crystals m-CzCN and p-CzCN as well as Lm-CzCN/m-BCzCN can be excited by visible light of 440 nm, showing 1–3 s afterglow due to the ordered molecular arrangement. The work not only provides a series of novel pure organic RTP materials, but also contributes to boost simple construction of efficient host-guest doping systems, as well as deep understanding of the structure-RTP function relationships.

CRediT authorship contribution statement

Jianmei Guo: Visualization, Validation, Software, Methodology, Investigation, Data curation. **Zhao Yupeng:** Visualization, Software. **Lei Ma:** Visualization, Supervision. **Yongtao Wang:** Writing – review & editing, Supervision, Conceptualization.

Declaration of competing interest

The authors declare that they have no known competing financial interests or personal relationships that could have appeared to influence the work reported in this paper.

Acknowledgement

This work was supported by the Guangxi Natural Science Foundation (Grant No. 2024GXNSFAA010423 and 2020GXNSFAA159147) and the National Natural Science Foundation of China (Grant No. 21766030).

Appendix A. Supplementary data

Supplementary data to this article can be found online at https://doi.org/10.1016/j.cjsc.2024.100335.

References

[1] M.-S. Gong, J.-R. Cha, C.W. Lee, Synthesis and device properties of mCP analogues based on fused-ring carbazole moiety, Org. Electron. 42 (2017) 66–74.
[2] L. Gu, H. Shi, M. Gu, K. Ling, H. Ma, S. Cai, L. Song, C. Ma, H. Li, G. Xing, X. Hang, J. Li, Y. Gao, W. Yao, Z. Shuai, Z. An, X. Liu, W. Huang, Dynamic ultralong organic phosphorescence by photoactivation, Angew. Chem. Int. Ed. 57 (2018) 8425–8431.
[3] C. Han, R. Du, H. Xu, S. Han, P. Ma, J. Bian, C. Duan, Y. Wei, M. Sun, X. Liu, W. Huang, Ladder-like energy-relaying exciplex enables 100% internal quantum efficiency of white TADF-based diodes in a single emissive layer, Nat. Commun. 12 (2021) 3640.
[4] M. Palner, K. Pu, S. Shao, J. Rao, Semiconducting polymer nanoparticles with persistent near-infrared luminescence for in vivo optical imaging, Angew. Chem. Int. Ed. 54 (2015) 11477–11480.
[5] K. Zhang, N. Dan, D.-D. Ren, R.-Y. Zhang, X. Lu, Y.-P. Wu, L.-L. Zhang, H.-R. Fu, D.-S. Li, A small D-A molecule with highly heat-resisting room temperature phosphorescence for white emission and anti-counterfeiting, Chin. J. Struct. Chem. 43 (2024) 100244.
[6] Y. Xie, Y. Ge, Q. Peng, C. Li, Q. Li, Z. Li, How the molecular packing affects the room temperature phosphorescence in pure organic compounds: ingenious molecular design, detailed crystal analysis, and rational theoretical calculations, Adv. Mater. 29 (2017) 1606829.
[7] Y. Su, S.Z.F. Phua, Y. Li, X. Zhou, D. Jana, G. Liu, W. Lim, W. Ong, C. Yang, Y. Zhao, Ultralong room temperature phosphorescence from amorphous organic materials toward confidential information encryption and decryption, Sci. Adv. 4 (2018) eaas9732.
[8] Z. An, C. Zheng, Y. Tao, R. Chen, H. Shi, T. Chen, Z. Wang, H. Li, R. Deng, X. Liu, W. Huang, Stabilizing triplet excited states for ultralong organic phosphorescence, Nat. Mater. 14 (2015) 685–690.
[9] O. Bolton, K. Lee, H.-J. Kim, K.Y. Lin, J. Kim, Activating efficient phosphorescence from purely organic materials by crystal design, Nat. Chem. 3 (2011) 205–210.
[10] Z. Yang, Z. Mao, X. Zhang, D. Ou, Y. Mu, Y. Zhang, C. Zhao, S. Liu, Z. Chi, J. Xu, Y.C. Wu, P.Y. Lu, A. Lien, M.R. Bryce, Intermolecular electronic coupling of organic units for efficient persistent room-temperature phosphorescence, Angew. Chem. Int. Ed. 55 (2016) 2181–2185.
[11] G. Zhang, G.M. Palmer, M.W. Dewhirst, C.L. Fraser, A dual-emissive-materials design concept enables tumour hypoxia imaging, Nat. Mater. 8 (2009) 747–751.
[12] Z.Y. Zhang, Y. Chen, Y. Liu, Efficient room-temperature phosphorescence of a solid-state supramolecule enhanced by cucurbit[6]uril, Angew. Chem. Int. Ed. 58 (2019) 6028–6032.
[13] N. Gan, X. Wang, H. Ma, A. Lv, H. Wang, Q. Wang, M. Gu, S. Cai, Y. Zhang, L. Fu, M. Zhang, C. Dong, W. Yao, H. Shi, Z. An, W. Huang, Manipulating the stacking of triplet chromophores in the crystal form for ultralong organic phosphorescence, Angew. Chem. Int. Ed. 58 (2019) 14140–14145.
[14] Y. Liu, Z. Ma, J. Liu, M. Chen, Z. Ma, X. Jia, Robust white-light emitting and multi-responsive luminescence of a dual-mode phosphorescence molecule, Adv. Opt. Mater. 9 (2020) 2001685.
[15] L. Gao, J. Huang, L. Qu, X. Chen, Y. Zhu, C. Li, Q. Tian, Y. Zhao, C. Yang, Stepwise taming of triplet excitons via multiple confinements in intrinsic polymers for long-lived room-temperature phosphorescence, Nat. Commun. 14 (2023) 7252.
[16] Q. Chen, L. Qu, H. Hou, J. Huang, C. Li, Y. Zhu, Y. Wang, X. Chen, Q. Zhou, Y. Yang, C. Yang, Long lifetimes white afterglow in slightly crosslinked polymer systems, Nat. Commun. 15 (2024) 2947.
[17] Z. Wang, L. Gao, Y. Zheng, Y. Zhu, Y. Zhang, X. Zheng, C. Wang, Y. Li, Y. Zhao, C. Yang, Four-in-One stimulus-responsive long-lived luminescent systems based on pyrene-doped amorphous polymers, Angew. Chem. Int. Ed. 61 (2022) e202203254.
[18] Y. Zhang, X. Chen, J. Xu, Q. Zhang, L. Gao, Z. Wang, L. Qu, K. Wang, Y. Li, Z. Cai, Y. Zhao, C. Yang, Cross-linked polyphosphazene nanospheres boosting long-lived organic room-temperature phosphorescence, J. Am. Chem. Soc. 144 (2022) 6107–6117.
[19] C. Wang, L. Qu, X. Chen, Q. Zhou, Y. Yang, Y. Zheng, X. Zheng, L. Gao, J. Hao, L. Zhu, B. Pi, C. Yang, Poly(arylene piperidine) quaternary ammonium salts

promoting stable long-lived room-temperature phosphorescence in aqueous environment, Adv. Mater. 34 (2022) 202204415.
[20] C. Wang, Y. Zhang, Z. Wang, Y. Zheng, X. Zheng, L. Gao, Q. Zhou, J. Hao, B. Pi, Q. Li, C. Yang, Y. Li, K. Wang, Y. Zhao, Photo-induced dynamic room temperature phosphorescence based on triphenyl phosphonium containing polymers, Adv. Funct. Mater. 32 (2022) 2111941.
[21] W. Gao, Z. Liu, X. Dai, W. Sun, Q. Gong, J. Li, Y. Ge, Color-tunable ultralong organic phosphorescence: commercially available triphenylmethylamine for UV-light response and anticounterfeiting, Chem. Asian J. 18 (2023) e202300450.
[22] Y. Gong, G. Chen, Q. Peng, W.Z. Yuan, Y. Xie, S. Li, Y. Zhang, B.Z. Tang, Achieving persistent room temperature phosphorescence and remarkable mechanochromism from pure organic luminogens, Adv. Mater. 27 (2015) 6195–6201.
[23] S. Jena, J. Eyyathiyil, S.K. Behera, M. Kitahara, Y. Imai, P. Thilagar, Crystallization induced room-temperature phosphorescence and chiral photoluminescence properties of phosphoramides, Chem. Sci. 13 (2022) 5893–5901.
[24] H. Wu, Y. Zhou, L. Yin, C. Hang, X. Li, H. Ågren, T. Yi, Q. Zhang, L. Zhu, Helical self-assembly-induced singlet-triplet emissive switching in a mechanically sensitive system, J. Am. Chem. Soc. 139 (2017) 785–791.
[25] X. Zhang, L. Du, W. Zhao, Z. Zhao, Y. Xiong, X. He, P.F. Gao, P. Alam, C. Wang, Z. Li, J. Leng, J. Liu, C. Zhou, J.W.Y. Lam, D.L. Phillips, G. Zhang, B.Z. Tang, Ultralong UV/mechano-excited room temperature phosphorescence from purely organic cluster excitons, Nat. Commun. 10 (2019) 5161.
[26] K. Zheng, X. Yang, F. Ni, Z. Chen, C. Zhong, C. Yang, Multicolor ultralong room-temperature phosphorescence from pure organic emitters by structural isomerism, Chem. Eng. J. 408 (2021) 127309.
[27] D. Li, F. Lu, J. Wang, W. Hu, X.-M. Cao, X. Ma, H. Tian, Amorphous metal-free room-temperature phosphorescent small molecules with multicolor photoluminescence via a host-guest and dual-emission strategy, J. Am. Chem. Soc. 140 (2018) 1916–1923.
[28] W. Qiu, X. Cai, M. Li, Z. Chen, L. Wang, W. Xie, K. Liu, M. Liu, S.-J. Su, Achieving purely organic room-temperature phosphorescence mediated by a host-guest charge transfer state, J. Phys. Chem. Lett. 12 (2021) 4600–4608.
[29] Y. Tian, J. Yang, Z. Liu, M. Gao, X. Li, W. Che, M. Fang, Z. Li, Multistage stimulus-responsive room temperature phosphorescence based on host-guest doping systems, Angew. Chem. Int. Ed. 60 (2021) 20259–20263.
[30] D. Wang, Y. Xie, X. Wu, Y. Lei, Y. Zhou, Z. Cai, M. Liu, H. Wu, X. Huang, Y. Dong, Excitation-dependent triplet-singlet intensity from organic host-guest materials: tunable color, white-light emission, and room-temperature phosphorescence, Phys. Chem. Lett. 12 (2021) 1814–1821.
[31] Y. Gong, J. Yang, M. Fang, Z. Li, Room-temperature phosphorescence from metal-free polymer-based materials, Cell Rep. Phys. Sci. 3 (2022) 100663.
[32] X. Shao, Molecular uniting set identified characteristic (MUSIC): a promising strategy for purely organic RTP luminogens, Sci. China Chem. 61 (2018) 975–976.
[33] Z. Yang, C. Xu, W. Li, Z. Mao, X. Ge, Q. Huang, H. Deng, J. Zhao, F.L. Gu, Y. Zhang, Z. Chi, Boosting the quantum efficiency of ultralong organic phosphorescence up to 52% via intramolecular halogen bonding, Angew. Chem. Int. Ed. 59 (2020) 17451–17455.
[34] Z. Zhou, Z. Song, J. Liu, B. Lei, J. Zhuang, X. Zhang, Y. Liu, C. Hu, Energy transfer mediated enhancement of room-temperature phosphorescence of carbon dots embedded in matrixes, Adv. Opt. Mater. 10 (2022) 2100704.
[35] N. Blagden, D.J. Berry, A. Parkin, H. Javed, A. Ibrahim, P.T. Gavan, L.L. De Matos, C.C. Seaton, Current directions in co-crystal growth, New J. Chem. 32 (2008) 1659–1672.
[36] H.-D. Wu, F.-X. Wang, Y. Xiao, G.-B. Pan, Preparation and ambipolar transistor characteristics of co-crystal microrods of dibenzotetrathiafulvalene and tetracyanoquinodimethane, J. Mater. Chem. C 1 (2013) 2286–2289.
[37] C. Demangeat, Y. Tang, Y. Dou, S. Dale, J. Cielo, E. Kim, H.J. Lee, A. D'Aléo, B. Hu, A.J. Attias, Necessary and sufficient condition for organic room-temperature phosphorescence from host-guest doped crystalline systems, Adv. Opt. Mater. 11 (2023) 2300289.
[38] X. Yan, H. Peng, Y. Xiang, J. Wang, L. Yu, Y. Tao, H. Li, W. Huang, R. Chen, Recent advances on host-guest material systems toward organic room temperature phosphorescence, Small 18 (2022) 2104073.
[39] A.C. Brannan, N. Le Phuoc, M. Linnolahti, A.S. Romanov, Organic persistent room temperature phosphorescence enabled by carbazole impurity, Front. Chem. 10 (2023) 1008658.
[40] C. Chen, Z. Chi, K.C. Chong, A.S. Batsanov, Z. Yang, Z. Mao, Z. Yang, B. Liu, Carbazole isomers induce ultralong organic phosphorescence, Nat. Mater. 20 (2021) 175–180.
[41] L. Yue, S. Yuan, Y. Zhang, Y. Wang, Q. Sun, H. Zhang, S. Xue, W. Yang, Gaining new insights into trace guest doping role in manipulating organic crystal phosphorescence, J. Phys. Chem. Lett. 12 (2021) 11616–11621.
[42] H. Xiao, D.S. Zheng, L.Y. Zhang, L.J. Xu, Z.N. Chen, Ultra-long room temperature phosphorescence with the efficiency over 64% induced by 1‰ impurity doping, Adv. Funct. Mater. 33 (2023) 2214241.
[43] B. Chen, X. Zhang, Y. Wang, H. Miao, G. Zhang, Aggregation-induced emission with long-lived room-temperature phosphorescence from methylene-linked organic donor-acceptor structures, Chem. Asian J. 14 (2018) 751–754.
[44] Z. Yin, M. Gu, H. Ma, X. Jiang, J. Zhi, Y. Wang, H. Yang, W. Zhu, Z. An, Molecular engineering through control of structural deformation for highly efficient ultralong organic phosphorescence, Angew. Chem. Int. Ed. 60 (2020) 2058–2063.
[45] J. Jiang, C. Hu, Y. Wang, L. Ma, J. Guo, Ultralong organic room-temperature phosphorescence, multiple stimulus responsiveness and high-level anti-counterfeiting based on multifunctional carbazolyl imidazolopyridine, Mater. Today Chem. 30 (2023) 101548.
[46] H. Liu, Q. Mu, X. Zhao, Y. Wang, Y. Song, L. Lin, C.-K. Wang, J. Fan, Theoretical perspective for structural isomerism effect on photoelectric properties of organic room temperature phosphorescence molecules, Mater. Today Chem. 34 (2023) 101814.
[47] Y. Liang, C. Xu, H. Zhang, S. Wu, J.A. Li, Y. Yang, Z. Mao, S. Luo, C. Liu, G. Shi, F. Sun, Z. Chi, B. Xu, Color-tunable dual-mode organic afterglow from classical aggregation-caused quenching compounds for white-light-manipulated anti-counterfeiting, Angew. Chem. Int. Ed. 62 (2023) e202217616.
[48] Y. Yang, Y. Liang, Y. Zheng, J.A. Li, S. Wu, H. Zhang, T. Huang, S. Luo, C. Liu, G. Shi, F. Sun, Z. Chi, B. Xu, Efficient and color-tunable dual-mode afterglow from large-area and flexible polymer-based transparent films for anti-counterfeiting and information encryption, Angew. Chem. Int. Ed. 61 (2022) e202201820.
[49] L. Hou, X. Yu, G. Wang, W. Huang, X. Zhu, H. Liu, L. Nie, W. Zhang, J. Qiu, X. Xu, T. Wang, Controllable ultralong phosphorescence through substituent modulation for dynamic anti-counterfeiting, Adv. Opt. Mater. 12 (2023) 202301812.